Characteristics of synchrotron Čerenkov radiation

R. Pratap,* K. Sasidharan, and Vinod Krishan
Indian Institute of Astrophysics, Bangalore 560 034, India
(Received 22 June 1992)

A diagrammatic technique has been worked out in the framework of nonequilibrium statistical mechanics as developed by Prigogine and co-workers to tackle the problem of radiation emission from a relativistic electron in an ambient plasma embedding an axial-wiggler magnetic field. The theory is exact in that the diagrams contributing towards the self-consistent-field approximation have been summed up exactly and one obtains a time-dependent response function. The kinetic regime has been obtained by eliminating the memory by taking an asymptotic limit in time. Explicit calculations have been affected to obtain functions like the Čerenkov angle and the refractive index as well as the power emitted by the system. It has been shown that the radiation emitted has very peculiar polarization features.

PACS number(s): 41.60.−m, 52.20.−j, 05.70.Ln, 95.30.Gv

I. INTRODUCTION

In a series of papers Rankin [1] and Rankin, Stinebring, and Weisberg [2] have very exhaustively collected almost all the known details of emission characteristics of pulsar radiation and have shown that these facts could be explained to a fair degree of accuracy by the model proposed by Radhakrishnan and Cook [3] for the Vela pulsar. Nearly complete lists of references up to 1989 are given in these papers. The radiations are expected to come from a cone centered around the magnetic axis of a neutron star rotating with an angular speed of 1000 rpm. This speed does not seem to be stationary in time. However, the patchy domains in the cone as depicted by Rankin [1] needs additional mechanisms to maintain an inhomogeneously structured magnetosphere in an axially symmetric dipole field.

We propose in this paper an alternate mechanism based on the Čerenkov process in a periodic magnetic field superposed on a constant field. The Čerenkov mechanism was already proposed by Bestin, Gurevich and Istomin [4] as a plausible radiation model for pulsars. However, the inclusion of an undulating magnetic field would drive the emission cone in an oscillatory process and produce what is known as the "search light" effect as in the free-electron-laser (FEL) dynamics. The trajectory of an electron together with its Čerenkov cone is shown in Fig. 1. The emission produced by the process is unpolarized, whereas the pulsar radiation shows significant polarization. Also, in the strong magnetic fields existing in such objects, nonlinear effects, such as curvature effects, as well as interaction between the synchrotron and Čerenkov processes resulting in a synergism, must play a very decisive role in the emission process, and hence any linear or a quasilinear theory including only one process or the other at a time would be inadequate to explain the features satisfactorily. Further, non-Markovian processes would be significant, which make the emission frequencies highly time dependent, which would result in a different kind of spectroscopy of these objects.

The model we propose here depends on the motion of a relativistic electron moving in a constant magnetic field which has been modulated by the very likely presence of a series of finite-amplitude magnetohydrodynamic (MHD) waves. This would result in a periodic field being imposed on the axial field. Such an arrangement is known as an axial-wiggler configuration. It was recently shown [5] that the Hamiltonian characterizing the motion of an electron in an axial-wiggler magnetic-field configuration can be made integrable through a series of canonical transformations. This, however, is in the absence of medium. The problem of the passage of a relativistic electron through a nonrelativistic plasma embedding an axial-wiggler field was solved recently [6,7] because of its importance in FEL dynamics, in the framework of nonequilibrium statistical mechanics as developed by Prigogine and co-workers [8]. In the astrophysical context, the ambient magnetic field very likely gets modified by the presence of finite-amplitude magnetohydrodynamic waves. These variations are in general time dependent and not necessarily periodic, but we consider this as static and spatially periodic in the first approximation, since the frequency of the MHD waves is much smaller than all the other frequencies in the system. The magnetic-field strength is represented by its cyclotron frequencies Ω_0 for the axial field and Ω for the wiggler field and the spatial undulation of the wiggler field by the wave vector k_w. The test particle is denoted

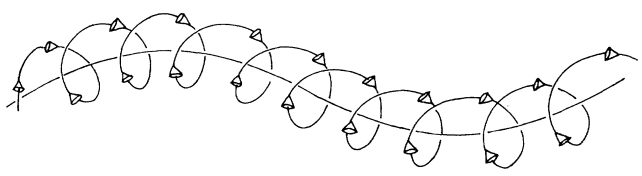

FIG. 1. Trajectory of a relativistic electron in an undulating magnetic field. The guiding center of the helical trajectory is anchored on the magnetic-field line. The cones represent the Čerenkov ones, with the electron at its apex.

by the suffix T, the plasma particles by 1. The system also has electromagnetic radiation characterized by λ. As the particle interacts with the radiation field (λ) and the medium particles together with the magnetic fields, we shall have four characteristic frequencies in the system, viz. ν_λ, $\omega_{\rm pl}$, Ω_0, and Ω, and therefore one should expect the emerging frequency as a synergic one [9,10] resulting in a masing action. The physical process in this is that the motion of the relativistic electron moving in the axial-wiggler field embedded in the quiescent plasma would generate synchrotron radiation due to the magnetic field, Čerenkov radiation due to plasma medium, and curvature radiation due to the spatial undulation of the wiggler field. The effective synchrotron frequency is given by $\bar{\Omega}=(\Omega_0^2+\Omega^2)^{1/2}$. The curvature radiation has the frequency $(v_z k_w)$. While the synchrotron radiation is polarized, the Čerenkov radiation is unpolarized. The dipole radiation generated by the plasma particles in the Čerenkov cone, together with the synchrotron and curvature radiations generated by the electrons, are partly absorbed by the electron that follows, thereby increasing its energy. This nonlinear interaction generates synergism or maser action. Hence the frequency of the emerging radiation will be unique and is a highly complicated function of these frequencies.

The paper is structured in the following manner. Section II gives the Hamiltonian formulation of the problem. The system consists of (i) a relativistic test particle (T), (ii) nonrelativistic plasma particles (l), and (iii) an ambient radiation field (λ) all in the presence of the axial-wiggler field, and we use the Hamiltonian of this system to evaluate the time derivatives appearing in the general Liouville equation in the $6N$-dimensional phase space. The formal solution of this equation is written in the characteristic coordinate system [Eq. (10)] and this solution is then transformed into the resolvant space [Eq. (16)]. Section III consists of a discussion of the noncommuting operators and the subsequent Baker-Hausdorff expansion. Section IV consists of a discussion of the terms appearing in Eq. (16) that contribute towards the self-consistent-field approximation which has coefficients of e^2n/m, e and m being electronic charge and mass, respectively, and n is the concentration in the thermodynamic limit $N\to\infty$, $V\to\infty$; $N/V=n$. The subset of infinite terms from the original Dyson series is summed up exactly, giving collective modes. Section V details the summation of the above series resulting in the response function in the one-particle distribution function (OPDF). Using this OPDF, we evaluate the average energy loss suffered by the test particle, and in the next section we obtain the expression for the Čerenkov angle as well as the refractive index [Eq. (57)]. In Sec. VII, we elaborate the Optics by discussing the refractive index, as in Sec. VIII we discuss the polarization. Section IX has a detailed discussion of the results evaluated from the above formulation. Section X lists the main conclusions. The evaluation of the response function is detailed in the Appendix.

II. FORMULATION OF THE PROBLEM

The system consists of a relativistic electron passing through a nonrelativistic plasma embedding an axial magnetic field (denoted by the cyclotron frequency Ω_0) and a wiggler field (Ω) acting as the inhomogeneous component. The system also has a radiation field with frequency ν_λ. The total Hamiltonian is written as

$$H=H_T+\sum_l H_l+\sum_\lambda H_\lambda \ , \tag{1}$$

where

$$\begin{aligned} H_T&=mc^2(1+u_T^2)^{1/2} \ , \\ H_l&=(1/2m_l)\left[P_l-\frac{e_l}{c}A^\lambda\right]^2 \ , \\ H_\lambda&=\sum_\lambda \nu_\lambda J_\lambda \ . \end{aligned} \tag{2}$$

In Eq. (2),

$$\begin{aligned} mc\,\mathbf{u}_T&=\tilde{\mathbf{P}}_T+\frac{m\Omega_0}{2}(\mathbf{j}x+\mathbf{i}y) \\ &\quad+\frac{m\Omega}{2k_w}(\mathbf{i}\cos k_w z+\mathbf{j}\sin k_w z)-\frac{e}{c}A_\lambda \ , \\ \mathbf{P}_l&=\tilde{\mathbf{P}}_l+\frac{m\Omega_0}{2}(\mathbf{i}y+\mathbf{j}x)+\frac{m\Omega}{2k_w}(\mathbf{i}\cos k_w z+\mathbf{j}\sin k_w z) \ . \end{aligned} \tag{3}$$

In Eq. (3), $\tilde{P}$ is the canonical momentum and k_w is the wave number of the wiggler field. All these are written in canonical variables. It may be noted that while u_T contain the interaction vector potential A_λ, P_l does not contain the same. Equation (2) may be expanded and the square term in A^λ will contribute (in the random-phase approximation [11]) an effective radiation frequency, $\bar{\nu}_\lambda=(\nu_\lambda^2+\omega_{\rm pl}^2)^{1/2}$, with $\omega_{\rm pl}$ being the plasma frequency. One can write Eq. (2) as

$$\begin{aligned} H_T&=mc^2(1+u_T^2)^{1/2} \ , \\ H_l&=\frac{1}{2m_l}P_l^2-(e_l/m_lc)(\mathbf{P}_l\cdot\mathbf{A}^\lambda) \ , \\ H_\lambda&=\sum_\lambda \bar{\nu}_\lambda J_\lambda \ . \end{aligned} \tag{4}$$

Here now $u_T=\beta_T/(1-\beta_T^2)^{1/2}$, which gives $(1+u_T^2)^{1/2}=(1-\beta_T^2)^{-1/2}=\gamma$. Hence the Hamiltonian for the relativistic particle is $mc^2\gamma$. We shall now write the continuity equation for the Liouville density,

$$\rho=\rho(\mathbf{q}_T,\mathbf{u}_T,\mathbf{q}_l,\mathbf{P}_l,J_\lambda,\omega_\lambda,t) \ , \tag{5}$$

as

$$\begin{aligned} &\frac{\partial\rho}{\partial t}+\dot{\mathbf{q}}_T\cdot\frac{\partial\rho}{\partial\mathbf{q}_T}+\dot{\mathbf{u}}_T\cdot\frac{\partial\rho}{\partial\mathbf{u}_T}+\dot{\mathbf{q}}_l\cdot\frac{\partial\rho}{\partial\mathbf{q}_l}+\dot{\mathbf{P}}_l\cdot\frac{\partial\rho}{\partial\mathbf{P}_l} \\ &\qquad+\dot{J}_\lambda\frac{\partial\rho}{\partial J_\lambda}+\dot{\omega}_\lambda\frac{\partial\rho}{\partial\omega_\lambda}=0 \ , \end{aligned} \tag{6}$$

and obtain the time derivatives appearing in Eq. (6) from the Hamiltonian equations. One can write Eq. (6) as

$$\frac{\partial\rho}{\partial t}+\mathcal{L}\rho=\exp(\delta L)\rho \ , \tag{7}$$

where now

$$\mathcal{L}=\mathcal{L}_T+\mathcal{L}_l+\mathcal{L}_\lambda \ , \tag{8}$$

with

$$\mathcal{L}_T=c\boldsymbol{\beta}_T\cdot\frac{\partial}{\partial \mathbf{q}_T}+\frac{\overline{\Omega}}{\gamma}\boldsymbol{\epsilon}_3\times\boldsymbol{\beta}_T\cdot\frac{\partial}{\partial\boldsymbol{\beta}_T} \ ,$$

$$\mathcal{L}_l=\frac{\mathbf{P}_l}{m_l}\cdot\frac{\partial}{\partial \mathbf{q}_l}+\overline{\Omega}\boldsymbol{\epsilon}_3\times\mathbf{P}_l\cdot\frac{\partial}{\partial\mathbf{P}_l} \ , \tag{9}$$

$$\mathcal{L}_\lambda=\overline{\nu}_\lambda\frac{\partial}{\partial\omega_\lambda} \ .$$

These operators are written in the natural coordinates of the system defined by the unit vectors $\boldsymbol{\epsilon}_1$, $\boldsymbol{\epsilon}_2$, and $\boldsymbol{\epsilon}_3$ as

$$\boldsymbol{\epsilon}_1=\frac{\Omega}{\overline{\Omega}}\hat{\mathbf{e}}_3+\frac{\Omega_0}{\overline{\Omega}}\hat{\mathbf{e}}_1=\frac{\Omega_0}{\overline{\Omega}}(i\cos k_w z+j\sin k_w z)+\frac{\Omega}{\overline{\Omega}}\mathbf{k} \ ,$$

$$\boldsymbol{\epsilon}_2=-i\sin k_w z+j\cos k_w z \ , \tag{10}$$

$$\boldsymbol{\epsilon}_3=\frac{\Omega_0}{\overline{\Omega}}\hat{\mathbf{e}}_3-\frac{\Omega}{\overline{\Omega}}\hat{\mathbf{e}}_1=-\frac{\Omega}{\overline{\Omega}}(i\cos k_w z+j\sin k_w z)+\frac{\Omega_0}{\overline{\Omega}}\mathbf{k} \ ,$$

where $\hat{\mathbf{e}}_1$, $\hat{\mathbf{e}}_2$, and $\hat{\mathbf{e}}_3$ are the wiggler coordinates and **i**, **j**, and **k** form the Cartesian system, $\overline{\Omega}^2=(\Omega_0^2+\Omega^2)$, and $\boldsymbol{\epsilon}_1$, $\boldsymbol{\epsilon}_2$, and $\boldsymbol{\epsilon}_3$ are Z dependent in the Cartesian system. But the Jacobian of transformation from Cartesian to wiggler systems as well as to the new coordinates is unity. All the terms in Eq. (6) containing A^λ are included in the (δL) operator, and this is defined as

$$(\delta L)=\mathcal{A}_T^\lambda+\mathcal{B}_T^\lambda+\mathcal{A}_l^\lambda+\mathcal{B}_l^\lambda \ , \tag{11}$$

where the operators are explicitly written as

$$\mathcal{A}_T^\lambda=\left[\frac{1}{m_T}(8/V\overline{\nu}_\lambda)^{1/2}a_\lambda\right]\frac{\partial}{\partial\mathbf{u}_T}\left[-\frac{\overline{\nu}_\lambda}{c}\mathbf{e}_\lambda(\sqrt{J_\lambda}\sin\omega_\lambda)\cos(\mathbf{K}_\lambda\cdot\mathbf{q}_T)+\boldsymbol{\beta}\times(\mathbf{K}_\lambda\times e_\lambda)(\sqrt{J_\lambda}\cos\omega_\lambda)\sin(\mathbf{K}_\lambda\cdot\mathbf{q}_T)\right] \ ,$$

$$\mathcal{A}_l^\lambda=\left[\frac{1}{m_l}(8/V\overline{\nu}_\lambda)^{1/2}a_\lambda\right]\left[\sqrt{J}\cos\omega_\lambda\left[\frac{\partial}{\partial\mathbf{q}_l}\cdot\mathbf{e}_\lambda+m\overline{\Omega}\frac{\partial}{\partial\mathbf{P}_l}\cdot(\boldsymbol{\epsilon}_3\times\mathbf{e}_\lambda)\right]\cos(\mathbf{K}_\lambda\cdot\mathbf{q}_l)\right] \ ,$$

$$\mathcal{B}_T^\lambda=\left[\left[\frac{8c^2}{V\overline{\nu}_\lambda}\right]^{1/2}a_\lambda\right]\left[(\boldsymbol{\beta}\cdot\mathbf{e}_\lambda)\cos(\mathbf{K}_\lambda\cdot\mathbf{q}_T)\sqrt{J_\lambda}\sin(\omega_\lambda)\frac{\partial}{\partial J_\lambda}\right] \ ,$$

$$\mathcal{B}_l^\lambda=\left[\frac{1}{m_l}\left[\frac{8}{V\overline{\nu}_\lambda}\right]^{1/2}a_\lambda\right]\left[(\mathbf{P}_l\cdot\mathbf{e}_\lambda\cos(\mathbf{K}_\lambda\cdot\mathbf{q}_l)\sqrt{J_\lambda}\sin(\omega_\lambda)\frac{\partial}{\partial J_\lambda}\right] . \tag{12}$$

In writing Eq. (12) we have used the expression for A_λ as

$$A_\lambda=\left[\frac{8c^2}{V\overline{\nu}_\lambda}\right]^{1/2}a_\lambda[e_\lambda(\sqrt{J_\lambda}\cos\omega_\lambda)\cos(\mathbf{K}_\lambda\cdot\mathbf{q})+e_\lambda(\sqrt{J_{-\lambda}}\cos(\omega_{-\lambda})\sin(\mathbf{K}_\lambda\cdot\mathbf{q})] \ . \tag{13}$$

In Eq. (12), a_λ is a dimensionless number denoting the strength of interaction, and in these operators we have written only the λ part. The $-\lambda$ part is obtained by replacing $\cos(\mathbf{K}_\lambda\cdot\mathbf{q})$ by $\sin(\mathbf{K}_\lambda\cdot\mathbf{q})$ and $\sin(\mathbf{K}_\lambda\cdot\mathbf{q})$ by $-\cos(\mathbf{K}_\lambda\cdot\mathbf{q})$. We have also retained only one term in the Poisson bracket, as we assume the initial distribution as angle independent.

We shall now make use of the linear nature of Eq. (7) and formally integrate, giving the general solution as

$$\rho(t)=e^{-\mathcal{L}t}\rho(0)+e\int_0^t d\tau\, e^{-\mathcal{L}(t-\tau)}(\delta L)\rho(\tau) \ , \tag{14}$$

where $\rho(0)$ is the initial state. Here the first term is the free flow term in which the initial state is transported to time t without any change, while the second term contains all of the interactions within the system. We shall now iterate Eq. (14) to get the general Dyson series as

$$\rho(t)=\sum_{n=0}^{\infty}e^n\int_0^t dt_1\int_0^{t_1}dt_2\cdots\int_0^{t_{n-1}}dt_n\, e^{-\mathcal{L}(t-t_1)}(\delta L)e^{-\mathcal{L}(t_1-t_2)}\cdots(\delta L)e^{-\mathcal{L}(t_{n-1}-t_n)}(\delta L)\times e^{-\mathcal{L}t_n}\rho(0) \ . \tag{15}$$

Equation (15) contains all of the information in the series and hence is the most general solution. It should be realized that Eq. (15) is not a perturbation series but is a general solution of the Liouville equation. We now pick up from this equation terms with (e^2c/m) as coefficients. It is interesting to note that the exponential operators in Eq. (15) have the time factor as $(t-t_1)$, $(t_1-t_2),\ldots,(t_{n-1}-t_n),t_n$ and since (δL) as well as $\mathcal{L}$ do not contain time explicitly, Eq. (15) is a convolution series, and hence in the resolvant space, this can be written as

$$\rho(t)=\frac{1}{2\pi}\sum_{n=0}^{\infty}e^n\int dz\, e^{-izt}R^0(z)[(\delta L)R^0(z)]^n\rho(0) \ , \tag{16}$$

where we have defined the Laplace transform as

$$\tilde{f}(z)=\frac{1}{2\pi}\int_0 e^{izt}f(t)dt \tag{17}$$

and $R(z)$ is the LT of the operator $e^{-\mathcal{L}\tau}$. The series (16) is a geometric progression and hence can be summed up exactly. In the next section some of the properties of these operators are discussed.

III. OPERATORS

The propagator $\exp(-\mathcal{L}\tau)$ has members which do not commute. When written explicitly,

$$-\tau\mathcal{L}=-(c\tau)\left[\beta\frac{\partial}{1\partial x}+\beta\frac{\partial}{2\partial y}+\beta\frac{\partial}{3\partial z}\right]+\left[\frac{\bar{\Omega}\tau}{\gamma}\right]\left[\beta\frac{\partial}{2\partial\beta_1}-\beta\frac{\partial}{1\beta_2}\right]. \tag{18}$$

In the new coordinate system with ε_3 in the Z direction, the second part of the operator corresponds to the angular momentum operator. Hence the operator (18) can be written as

$$-\mathcal{L}\tau=-c\tau\beta_\rho\left[\cos\theta\frac{\partial}{\partial x}+\sin\theta\frac{\partial}{\partial y}\right]-(\beta_3 c\tau)\frac{\partial}{\partial z}-\frac{\bar{\Omega}\tau}{\gamma}\frac{\partial}{\partial\theta}. \tag{19}$$

We shall affect a Baker-Hausdorff expansion of these noncommuting operators appearing in the propagator following Fujiwara [12].

We now define

$$A=-\frac{\bar{\Omega}\tau}{\gamma}\frac{\partial}{\partial\theta},\qquad B=-c\tau\beta_\rho\left[\cos\theta\frac{\partial}{\partial x}+\sin\theta\frac{\partial}{\partial y}\right], \tag{20}$$

$$e^{-\mathcal{L}\tau}=e^{A+B}=e^{A}\exp\int_0^1 d\lambda\left[B-\lambda[A,B]+\frac{\lambda^2}{2!}[A,[A,B]]-\frac{\lambda^3}{3!}[A,[A,[A,B]]]+\cdots\right], \tag{21}$$

where the square bracket is a commutator. Since γ is $(1-\beta^2)^{-1/2}$ it is independent of θ and

$$[A,B]=\left[\frac{\bar{\Omega}\tau}{\gamma}\right]B^*,\qquad B^*=c\tau\beta_\rho\left[-\sin\theta\frac{\partial}{\partial x}+\cos\theta\frac{\partial}{\partial y}\right], \tag{22}$$

$$[A,[AB]]=-\left[\frac{\bar{\Omega}\tau}{\gamma}\right]^2 B. \tag{23}$$

Hence Eq. (21) becomes

$$e^{-\mathcal{L}\tau}=e^{(\bar{\Omega}\tau/\gamma)(\partial/\partial\theta)}\exp\left\{\frac{c\gamma}{\bar{\Omega}}\left[\beta_1\sin\frac{\bar{\Omega}\tau}{\gamma}+\beta_2\left[1-\cos\frac{\bar{\Omega}\tau}{\gamma}\right]\right]\frac{\partial}{\partial x}-\frac{c\gamma}{\Omega}\left[\beta_2\sin\frac{\bar{\Omega}\tau}{\gamma}-\beta_1\left[1-\cos\frac{\bar{\Omega}\tau}{\gamma}\right]\right]\frac{\partial}{\partial y}-(\beta_3 c\tau)\frac{\partial}{\partial z}\right\}. \tag{24}$$

If, now, we measure the length in terms of $(\hbar/m\Omega_0)^{1/2}$ and momentum in units of $(m\hbar\Omega_0)^{1/2}$, we can write Eq. (24) as

$$e^{-\mathcal{L}\tau}=\exp\left[-\frac{\alpha\Omega_0}{\omega}[\beta_1\sin\omega\tau+\beta_2(1-\cos\omega\tau)]\frac{\partial}{\partial\xi}+\frac{\alpha\Omega_0}{\omega}[\beta_1(1-\cos\omega\tau)-\beta_2\sin\omega\tau]\frac{\partial}{\partial\eta}-\alpha\Omega_0\beta_3\tau\frac{\partial}{\partial\zeta}\right]e^{-\omega\tau(\partial/\partial\theta)} \tag{25}$$

where

$$\alpha=\left[\frac{mc^2}{\hbar\Omega_0}\right]^{1/2},\quad \omega=\bar{\Omega}/\gamma,\quad \beta_1=\beta_\rho\cos\theta,\quad \beta_2=\beta_\rho\sin\theta,\quad \begin{Bmatrix}x\\y\\z\end{Bmatrix}=\left[\frac{\hbar}{m\Omega_0}\right]^{1/2}\times\begin{Bmatrix}\xi\\\eta\\\zeta\end{Bmatrix}.$$

A similar procedure for the operator corresponding to the field particles would give

$$e^{-\mathcal{L}_I\tau}=\exp\left[-\frac{\Omega_0}{\bar{\Omega}}(P_1\sin\bar{\Omega}\tau+P_2(1-\cos\bar{\Omega}\tau)\frac{\partial}{\partial\xi}+\frac{\Omega_0}{\Omega}(P_1(1-\cos\bar{\Omega}\tau)-P_2\sin\bar{\Omega}\tau)\frac{\partial}{\partial\eta}-P_3\Omega_0\tau\frac{\partial}{\partial\zeta}\right]e^{-\bar{\Omega}\tau(\partial/\partial\theta)}, \tag{26}$$

where

$$P_1=P_\rho\cos\theta,\quad P_2=P_\rho\sin\theta.$$

This completes the Baker-Hausdorff expansion of the propagator.

IV. MATRIX ELEMENTS OR "DIAGRAMS" IN EQ. (15)

We shall next consider the right-hand side of Eq. (15). One can write the integrand as

$$\theta_n=e^{i\mathcal{L}t_1}(\mathcal{A}_\lambda^T+\mathcal{B}_\lambda^T+\mathcal{A}_\lambda^I+\mathcal{B}_\lambda^I)\theta'_{n-1}, \tag{27}$$

where

$$\theta'_{n-1}=e^{-i\mathcal{L}(t_1-t_2)}(\delta L)e^{-i\mathcal{L}(t_2-t_3)}\cdots(\delta L)e^{-i\mathcal{L}t_n} . \quad (28)$$

The $\mathcal{B}$ operators are Poisson brackets, and making use of a well-known property of Poisson bracket

$$\int dx\,dy\{U,V\}=0 ,$$

where U and V are functions vanishing at the boundary, we see that in Eq. (27) only an A vertex can appear on the extreme left and that a B vertex will always succeed an A vertex. With this result, we shall consider few terms of the series. Furthermore, since we are integrating over the field particle variables, the series necessarily have to start with an A^T vertex.

(a) The first term is when $n=1$ and this can be written as

$$e\int_0^t dt_1\int dJ_\lambda d\omega_\lambda e^{i\mathcal{L}t_1}\mathcal{A}^T_\lambda e^{-i\mathcal{L}t_1}\rho(0) , \quad (29)$$

and this term would vanish on integration of action angle variables of the radiation field, since the vertex A has a $\cos\omega_\lambda$ term. Thus the first-order term would vanish.

(b) The second-order term is written as

$$e^2\int_0^t dt_1\int_0^{t_1} dt_2 e^{i\mathcal{L}t_1}\mathcal{A}^T_\lambda e^{-i\mathcal{L}(t_1-t_2)} \times(\mathcal{A}^T_{\lambda'}+\mathcal{B}^T_{\lambda'}+\mathcal{A}^l_{\lambda'}+\mathcal{B}^l_{\lambda'})e^{-\mathcal{L}t_2}\rho(0) , \quad (30)$$

where λ and λ' could in general be different. However, on integration over ω_λ and J_λ we get a nonvanishing contribution only when $\lambda=\lambda'$. Since the field particle indices are integrated out, A^l and B^l terms would vanish and so also $\mathcal{A}^T_\lambda$ would vanish on λ integration. Hence the only term left is

$$\int_0^t dt_1\int_0^{t_1} dt_2 e^{(\mathcal{L}_T+\mathcal{L}_l)t_1}\mathcal{A}^T_\lambda e^{-(\mathcal{L}_T+\mathcal{L}_l)(t_1-t_2)} \times\mathcal{B}^T_\lambda e^{-(\mathcal{L}_T+\mathcal{L}_l)t_2}\rho(0) . \quad (31)$$

In this the propagator $e^{\mathcal{L}_l\tau}$ would be unity as l variables are integrated. We ultimately get

$$\int_0^t dt_1\int_0^{t_1} dt_2 e^{+\mathcal{L}_T t_1}\mathcal{A}^T_\lambda e^{-\mathcal{L}_T(t_1-t_2)}\mathcal{B}^T_\lambda e^{-\mathcal{L}_T t_2}\rho_T(0) , \quad (32)$$

and this is represented Fig. 2. The figure has to be read from right to left. The solid line is the propagator $e^{-\mathcal{L}_T t_2}$ which takes $\rho_T(0)$ from 0 to t_2. At t_2 a B vertex creates a correlation by emitting a virtual photon of wavelength (λ) and both these are propagated from t_2 to t_1, the test particle along the upper line and the radiation by the lower dashed line. At t_1 the particle absorbs this radiation and is propagated along $e^{-\mathcal{L}(t-t_1)}$ to t. This now is said to have completed an interaction with the field. In the above, a circle represents an A vertex and a square a B vertex. The interaction starts at t_2, creating a correlation by the vertex B and is annihilated at t_1 by the vertex A. This is the first nonzero term.

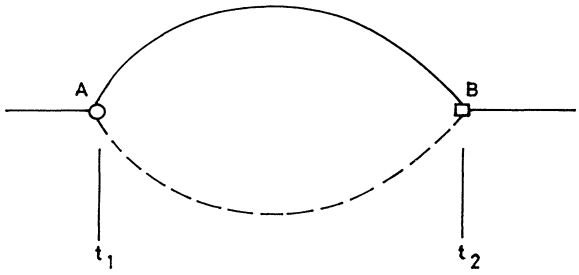

FIG. 2. The interaction of the particle with the radiation field. The solid curve in the upper part depicts the test particle and the slashed curve at the bottom represents a photon. The square denotes a creation vertex (B) and the circle an annihilation vertex (A). The diagram has to be read from right to left. The state is taken from zero to t_2 by the propagator at which a virtual photon is emitted which is absorbed at t_1 and finally propagated to t.

The third-order term also vanishes for the same reason as the first order. The fourth-order terms are given as

$$\int_0^t dt_1\int_0^{t_1} dt_2\int_0^{t_2} dt_3\int_0^{t_3} dt_4 e^{\mathcal{L}t_1}\mathcal{A}^T_\lambda e^{-\mathcal{L}(t_1-t_2)}(\mathcal{A}^T_{\lambda'}+\mathcal{B}^T_{\lambda'}+\mathcal{A}^l_{\lambda'}+\mathcal{B}^1_{\lambda'})e^{-\mathcal{L}(t_2-t_3)}(\mathcal{A}^T_{\lambda''}+\mathcal{B}^T_{\lambda''}+\mathcal{A}^l_{\lambda''}+\mathcal{B}^l_{\lambda''}) \times e^{-\mathcal{L}(t_3-t_4)}(\mathcal{A}^T_{\lambda'''}+\mathcal{B}^T_{\lambda'''}+\mathcal{A}^l_{\lambda'''}+\mathcal{B}^l_{\lambda'''})e^{-\mathcal{L}t_4}\rho(0) . \quad (33)$$

If we pick up only the terms in which the test particles are involved, we get the situation shown in Fig. 3. These are the only three possibilities in which the test particle is involved. As there are no field particles participating in this, there will be two orders of volume appearing in the matrix element. One volume factor would be absorbed in the summation over K_λ as $(8\pi^3/V)\sum K_\lambda\to\int dK_\lambda$, while the other volume (inverse) would set the first and second terms as vanishing in taking the thermodynamic limit. In the last one, the two terms are identical, and they have already been accounted for when we take the first term. This completes the operators with only the test particle vertices. The remaining terms give different possibilities depending on the position of these vertices in the time sequence. However, the nonvanishing terms are given as follows:

$$e^{-\mathcal{L}(t-t_1)}\mathcal{A}^T_\lambda e^{-\mathcal{L}(t_1-t_2)}\mathcal{B}^1_\lambda \times e^{-\mathcal{L}(t_2-t_3)}\mathcal{A}^l_{\lambda'}e^{-\mathcal{L}(t_3-t_4)}\mathcal{B}^T_{\lambda'} , \quad (34a)$$

$$e^{-\mathcal{L}(t-t_1)}\mathcal{A}^T_\lambda e^{-\mathcal{L}(t_1-t_2)}\mathcal{A}^T_{\lambda'} \times e^{-\mathcal{L}(t_2-t_3)}\mathcal{B}^l_\lambda e^{-\mathcal{L}(t_3-t_4)}\mathcal{B}^l_{\lambda'} , \quad (34b)$$

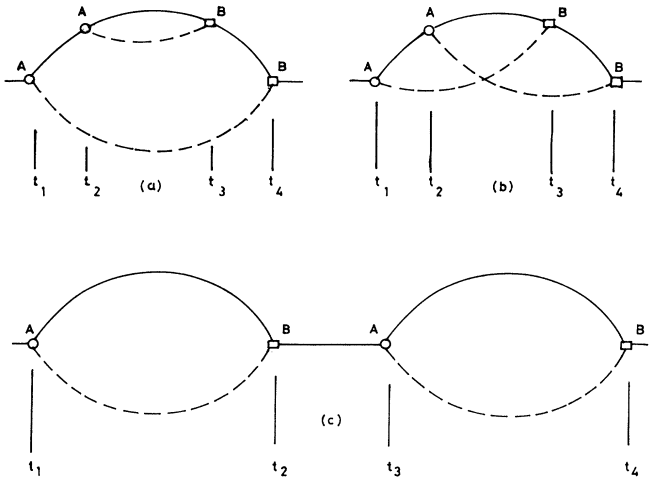

FIG. 3. The various possibilities of fourth-order interaction between the test particle and the radiation field, the order being denoted by the power of e.

$$e^{-\mathcal{L}(t-t_1)}\mathcal{A}_\lambda^T e^{-\mathcal{L}(t_1-t_2)}\mathcal{B}_\lambda^l \times e^{-\mathcal{L}(t_2-t_3)}\mathcal{A}_{\lambda'}^T e^{-\mathcal{L}(t_3-t_4)}\mathcal{B}_{\lambda'}^l , \quad (34c)$$

$$e^{-\mathcal{L}(t-t_1)}\mathcal{A}_\lambda^l e^{-\mathcal{L}(t_1-t_2)}\mathcal{A}_{\lambda'}^T \times e^{-\mathcal{L}(t_2-t_3)}\mathcal{B}_{\lambda'}^l e^{-\mathcal{L}(t_3-t_4)}\mathcal{B}_\lambda^l , \quad (34d)$$

and these are repreented in Figs. 4(a)–4(d). In Fig. 4(a) the particle emits a photon at t_4 which is absorbed by a field particle at t_3 which is again emitted at t_2 and finally absorbed by the test particle at t_1. In Fig. 4(b) the field particle emits photons at t_4 and again at t_3 and these are absorbed by the test particles at t_2 and t_1, respectively. All of these diagrams give rise to distinct series.

We shall now consider density dependence. Wherever a particle index 1 appears, one has to sum over them, thereby getting N. In Fig. 3, there are four vertices and hence $1/V^2$. Conservation of wave vectors gives only one K_λ, and after making the above transformation, we are still left with $1/V$. As there are no field particles involved in the above interaction, this matrix element would vanish on taking the limit $V\to\infty$. All of the figures [4(a)–4(b)] are 4-vertex diagrams. However, there is a field particle involved in this which gives a factor N, which in the thermodynamic limit would give a concentration n_0. Here, these diagrams are of the order

$$e^2\left[\frac{e^2 n_0}{m_l m_T}\right]\to\left[\frac{e^2}{m_T}\omega_{\rm pl}^2\right] .$$

All of the subsequent terms would be $(e^2/m_T)(\omega_{\rm pl}^2)^n$, where n gives the number of field particles involved. We are now ready to sum the series and obtain the collective modes. We now consider the subset of diagrams from Dyson series (15) with coefficients containing the interaction time scale $(m/e^2c)^{1/2}$, and this constitutes the self-consistent-field approximation. We thus get

$$\rho(t)=\langle T_f|T_i\rangle+\langle T_f|\delta L|x\rangle\langle x|\delta L|T_i\rangle+\cdots = \left\langle T_f\left|\oint e^{-izt}\frac{1}{1-\varepsilon(z)}\right|T_i\right\rangle , \quad (35)$$

where $\langle T_f|$ and $|T_i\rangle$ are the final and initial states, re-

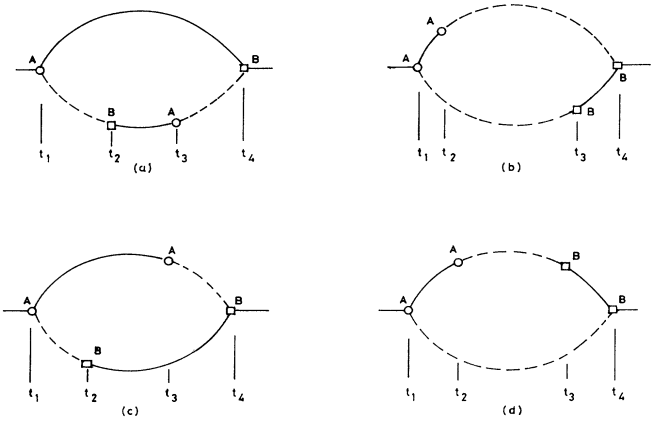

FIG. 4. (a)–(d) are the various interaction possibilities of the test particle through a radiation field with one field particle. The different possiblities are due to the position of the vertices with respect to time.

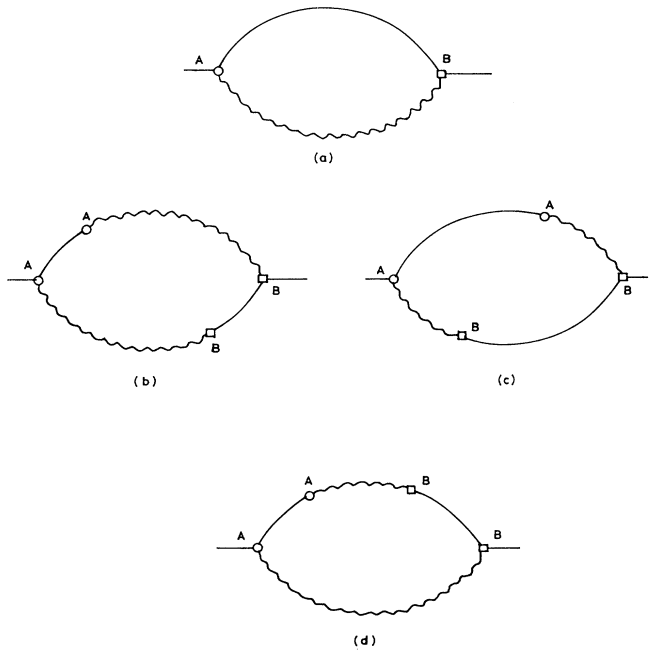

FIG. 5. Collective interaction to which the test particle is subjected by the medium and the photon field. Each diagram of Fig. 4 gives its own collective mode. While Fig. 4(a) gives a single response function (single wiggly line). (b)–(d) give two collective modes. This is due to the binary mixture of the interaction.

spectively, of the test particle, and this can be written as

$$\rho(t)=e^2\int_0^t dt_1\int_0^{t_1} dt_2 e^{-\mathcal{L}(t-t_1)}\mathcal{A}_\lambda^T e^{-\mathcal{L}(t_1-t_2)} \times\left[\oint dz\, e^{-iz(t_1-t_2)}u(z)\frac{1}{1-\varepsilon(z)}\right] \times\mathcal{B}_\lambda^T e^{-\mathcal{L}t_2}\rho_T(0)\ , \tag{36}$$

where

$$u(z)=\frac{iz}{z^2-\nu_\lambda^{-2}}$$

and $\varepsilon(z)$, the response function, is given in the Appendix. The diagram corresponding to Eq. (36) is shown in Fig. 5(a), where the curly line is represented in Fig. 6. We do get similar diagrams for the other terms appearing in Eq. (34). These are given in Figs. 5(b)–5(d).

This completes the collective interaction in a plasma.

FIG. 6. Diagram representing the series (35) resulting in the collective mode.

It may be noted that while in Fig. 5(a), the is only one response function, for Figs. 5(b)–5(d) there are two response functions corresponding to the two segments of the curly lines in them. This corresponds to two distinct collective modes and arises because of the binary nature of elementary interaction. We shall consider the single-particle distribution function as given by Fig. 5(a).

V. THE ONE-PARTICLE DISTRIBUTION FUNCTION (ODPF)

In evaluating any local property, we require a OPDF. Substituting the operators in Eq. (36), we can write the ODPF as

$$f(t)=\left[\frac{8\pi e^2}{mV}a_\lambda^2\right]\sum_{K_\lambda}\int_0^t dt_1\int_0^{t_1} dt_2\frac{\partial}{\partial\mathbf{u}}\cdot\mathbf{e}_\lambda(\mathbf{e}_{\lambda'}\cdot\bar{\boldsymbol{\beta}})\cos[(\mathbf{K}_{\lambda'}-\mathbf{K}_\lambda)\cdot\mathbf{q}_T+\phi] \times e^{-\mathcal{L}t_2}\rho_T(0)\oint dz\, e^{-izt_{12}}\frac{iz}{(z^2-\bar{\nu}_\lambda^2)}\frac{1}{\left[1-\dfrac{\chi(0)}{(z^2-\bar{\nu}_\lambda^2)(z^2-\bar{\Omega}^2)}\right]}\ , \tag{37}$$

where

$$\bar{\beta}=\beta\cos\omega t_{12}+\beta\epsilon_3\sin\omega t_{12}+\epsilon_3(\boldsymbol{\beta}\cdot\boldsymbol{\epsilon}_3)(1-\cos\omega t_{12})\ , \tag{38}$$

$$\phi=\frac{\alpha\Omega_0}{\omega}[\boldsymbol{\epsilon}_3\cdot\boldsymbol{\beta}\times\mathbf{K}_\lambda(1-\cos\omega t_{12})-(\mathbf{k}_\lambda\cdot\boldsymbol{\beta})\sin\omega t_{12}] +(\boldsymbol{\epsilon}_3\cdot K_\lambda)(\boldsymbol{\epsilon}_3\cdot\boldsymbol{\beta})(\sin\omega t_{12}-\omega t_{12})\ ,$$

with

$$\omega=\frac{\bar{\Omega}}{\gamma},\quad t_{12}=t_1-t_2,\quad \alpha=\left[\frac{mc^2}{\hbar\Omega_0}\right]^{1/2}. \tag{39}$$

In writing Eq. (37) we have taken into account the $-\lambda$ part as well. We shall convert the summation over $\mathbf{K}_\lambda$ into integration. Also we shall consider the wave-vector conservation $\mathbf{K}_\lambda-\mathbf{K}_\lambda=\boldsymbol{\epsilon}_1 l$ and the corresponding new polarization $\mathbf{e}_{\lambda'}=\mathbf{e}_\lambda-\boldsymbol{\epsilon}_3[(\mathbf{e}_1\cdot\mathbf{e}_\lambda)/(\mathbf{K}_\lambda\cdot\boldsymbol{\epsilon}_3)]l$ such that $\mathbf{e}_{\lambda'}\cdot\mathbf{K}_{\lambda'}=0$ if $\mathbf{e}_\lambda\cdot\mathbf{K}_\lambda=0$. With this, Eq. (37) takes the form

$$f(t)=\frac{e^2a_\lambda^2}{2m\pi^2}\int dK_\lambda\int_0^t dt_1\int_0^{t_1} dt_2\frac{\partial}{\partial\mathbf{u}}\cdot\mathbf{e}_\lambda(\mathbf{e}_{\lambda'}\cdot\bar{\boldsymbol{\beta}})\cos(1\xi+\phi)e^{-\mathcal{L}t_2}\rho_T(0) \times\oint dz\, e^{-izt_{12}}\left[\left[1+\frac{\bar{\nu}_\lambda^2-\bar{\Omega}^2}{\sigma}\right]\frac{iz}{z^2-[(\bar{\nu}_\lambda^2+\bar{\Omega}^2+\sigma)/2]} +\left[1-\frac{\bar{\nu}_\lambda^2-\bar{\Omega}^2}{\sigma}\right]\frac{iz}{z^2-[(\bar{\nu}_\lambda^2+\bar{\Omega}^2-\sigma)/2]}\right], \tag{40}$$

where

$$\sigma^2=(\bar{\nu}_\lambda^2-\bar{\Omega}^2)^2+4\chi(0)\ . \tag{41}$$

We can take now the inverse Laplace transform of Eq. (40), and it is observed that the effective frequency of emission is $[(\bar{\nu}_\lambda^2+\bar{\Omega}^2\mp\sigma)/2]^{1/2}$. For cases $\bar{\nu}_\lambda^2+\bar{\Omega}^2<\sigma$ this frequency becomes imaginary and we get absorption.

VI. AVERAGE ENERGY LOSS BY THE TEST PARTICLE

We shall now evaluate the average rate of loss of energy by averaging the test particle Hamiltonian using Eq. (40) and the derivative, finding its time. We, thus, have after a partial integration

$$\frac{d\bar{E}}{dt}=\left[\frac{e^2a_\lambda^2c^2}{2\pi^2}\right]\int d\mathbf{K}_\lambda\int_0^t dt_2(\mathbf{e}_\lambda\cdot\boldsymbol{\beta})(\mathbf{e}_{\lambda'}\cdot\bar{\boldsymbol{\beta}})\cos(1\xi+\phi)e^{-\mathcal{L}t_2}\rho_T(0)$$
$$\times\left[\left[1+\frac{\bar{\nu}_\lambda^2-\bar{\Omega}^2}{\sigma}\right]\cos\sqrt{(\bar{\nu}_\lambda^2+\bar{\Omega}^2+\sigma)/2}(t-t_2)\right.$$
$$\left.+\left[1-\frac{\bar{\nu}_\lambda^2-\bar{\Omega}^2}{\sigma}\right]\cos\sqrt{(\bar{\nu}_\lambda^2+\bar{\Omega}^2-\sigma)/2}(t-t_2)\right]. \tag{42}$$

We shall construct an initial state from the wave functions of the Klein-Gordon equation without the interaction potential, weighted with the Boltzmann function as

$$\rho(0)=\sum_{n,m}\langle\varphi_m|e^{-\beta H_0}|\varphi_n\rangle$$
$$=\sum_n\frac{H_n^2(\xi+\beta_2)}{2^n n!\sqrt{\pi}}e^{-(\beta_2+\xi)^2}e^{-\beta E_n}\delta(\eta)\delta(\xi)\delta(\beta_\rho)\delta(\beta_3-\beta_0), \tag{43}$$

where the eigenvalues $E_n=mc^2+[(n+1/2)+(P_3^2/2)\hbar\Omega_0$. We shall substitute this in Eq. (42), transform u integrations to β integration by writing $du=\gamma^5 d\boldsymbol{\beta}$, and perform ξ,η integrations, and after summing over the Landau levels, we get

$$\frac{d\bar{E}}{dt}=\left[\frac{e^2c^2}{2\pi^2}\Gamma\right]\int d\mathbf{K}_\lambda\int d\boldsymbol{\beta}\int d\zeta\int_0^t dt_2(\mathbf{e}_\lambda\cdot\boldsymbol{\beta})(\mathbf{e}_{\lambda'}\cdot\bar{\boldsymbol{\beta}})\cos\bar{\phi}\,\delta(\zeta-\alpha\Omega_0\beta_3 t_2)\delta(\beta_\rho)$$
$$\times\delta(\beta_3-\beta_0)\left[\left[1+\frac{\bar{\nu}_\lambda^2-\bar{\Omega}^2}{\sigma}\right]\cos\sqrt{(\bar{\nu}_\lambda^2+\bar{\Omega}^2+\sigma)/2}(t-t_2)\right], \tag{44}$$

where now

$$\bar{\phi}=\frac{\alpha\Omega_0}{\omega}[(\beta_1K_2-\beta_2K_1)(1-\cos\omega t_{12})-(\beta_1K_1+\beta_2K_2)\sin\omega t_{12}]$$
$$+1\left[-\beta_2+\left[1+\frac{\alpha\Omega_0}{\omega}\right](\beta_1\sin\omega t_2+\beta_2(1-\cos\omega t_2)\right]-(\alpha\beta_3K_3\Omega_0)t_{12},$$
$$\Gamma=\gamma^5a_\lambda^2\frac{e^{-(1^2/4)\coth(\beta\hbar\Omega_0/2)}}{2\sinh\dfrac{\beta\hbar\Omega_0}{2}}. \tag{45}$$

We now perform the β integration and get Eq. (44) as

$$\frac{d\bar{E}}{dl}=\left[\frac{e^2\Gamma}{2\pi^2c^2}\beta_0^2\right]\int_0^t dt_2\int\nu_\lambda^2 d\nu_\lambda d\mu\,d\phi\int d\zeta\left[(1-\mu^2)-\frac{1}{K_\lambda}\sin\theta\cos\phi\right]$$
$$\times\cos(\alpha K_\lambda\beta_0\Omega_0\mu\overline{t-t_2})\left[1+\frac{\bar{\nu}_\lambda^2-\bar{\Omega}^2}{\sigma}\right]$$
$$\times\cos\sqrt{(\bar{\nu}_\lambda^2+\bar{\Omega}^2+\sigma)/2}\overline{t-t_2}\,\delta(\zeta-\beta_0\Omega_0t_2). \tag{46}$$

Equation (46) contains two terms as far as the propagation vector is concerned, the second one depending on the azimuthal angle ϕ. We have expressed $\mathbf{K}_\lambda$ in spherical polar coordinates. Again from the δ functions, it becomes obvious that ζ has a range from 0 to $\beta_0\Omega_0 t$. We can now perform t_2 integration and write the power radiated per unit length as a function of time after integrating over t_2 as

$$\frac{d\bar{E}}{dl}=\left[\frac{e^2\Gamma\beta_0}{c^24\pi\Omega_0}\right]\int\nu_\lambda^2 d\nu_\lambda d\mu\int d\zeta(1-\mu^2)\left[1+\frac{\bar{\nu}_\lambda^2-\bar{\Omega}^2}{\sigma}\right]$$
$$\times\left[\cos(\alpha K_\lambda\beta_0\Omega_0\mu+\sqrt{(\bar{\nu}_\lambda^2+\bar{\Omega}^2+\sigma)/2})\left[t-\frac{\zeta}{\beta_0\Omega_0}\right]\right.$$
$$\left.+\cos(\alpha K_\lambda\beta_0\Omega_0\mu-\sqrt{(\bar{\nu}_\lambda^2+\bar{\Omega}^2\sigma)/2})\left[t-\frac{\zeta}{\beta_0\Omega_0}\right]\right]. \tag{47}$$

Integrating over ζ and taking asymptotic limit in time, Eq. (47) takes the form

$$\frac{d^2\bar{E}}{dl\,d\Omega}=\left[\frac{e^2\Gamma\beta_0^2}{4\pi^2c^2}\right]\int v_\lambda^2 dv_\lambda d\mu(1-\mu^2)\left[1+\frac{\bar{v}_\lambda^2-\bar{\Omega}^2}{\sigma}\right]$$
$$\times[\delta[\alpha\Omega_0\mathbf{K}_\lambda\beta_-\mu+\sqrt{(\bar{v}_\lambda^2+\bar{\Omega}^2+\sigma)/2}]+\delta(\alpha\Omega_0\mathbf{K}_\lambda\beta_0\mu-\sqrt{(\bar{v}_\lambda^2+\bar{\Omega}^2+\sigma)/2})]\ , \tag{48}$$

which gives the resonance condition, thereby giving the usual Čerenkov angle as

$$\mu=\mp\left[\frac{\bar{v}_\lambda^2+\bar{\Omega}^2+\sigma}{2\beta_0^2\bar{v}_\lambda^2}\right]^{1/2}\ . \tag{49}$$

If we now integrate Eq. (48) over μ, we get

$$\frac{d^2\bar{E}}{dl\,d\Omega}=\frac{e^2\Gamma\beta_0}{4\pi^2c^2}\int v_\lambda dv_\lambda\left[1+\frac{\bar{v}_\lambda^2-\bar{\Omega}^2}{\sigma}\right]$$
$$\times\left[1-\frac{\bar{v}_\lambda^2+\bar{\Omega}^2+\sigma}{2\beta_0^2\bar{v}_\lambda^2}\right]\ . \tag{50}$$

One can realize from the definition of σ in Eq. (41), that

$$2\bar{v}_\lambda d\bar{v}_\lambda\left[1+\frac{\bar{v}_\lambda^2-\bar{\Omega}^2}{\sigma}\right]=d(\bar{v}_\lambda^2+\bar{\Omega}^2+\sigma)=d\omega^2\ , \tag{51}$$

and with this Eq. (50) can be written as

$$\frac{d^2\bar{E}}{dl\,d\Omega}=\frac{e^2\Gamma}{c^2}\int\omega\,d\omega\left[1-\frac{\omega^2}{2\beta_0^2\bar{v}_\lambda^2}\right]$$
$$=\frac{e^2\Gamma}{c^2}\int\omega\,d\omega\left[1-\frac{1}{\beta_0^2N^2}\right]\ , \tag{52}$$

where

$$N^2=1+\frac{2\chi 1}{\bar{\Omega}^2\omega^2}+\frac{2\chi}{\bar{\Omega}^2}\frac{1}{2\bar{\Omega}^2-\omega^2}\ . \tag{53}$$

Equation (52) is the form of the Čerenkov conditions as given by Frank & Tamm [13].

VII. OPTICS OF THE SYSTEM

Equation (53) gives the refractive index of the medium. This consists of three terms: the first is that of vacuum, the second is the refractive index of the photon gas with the effective frequency as given by Eq. (51), while the third depends on the shifted frequency due to synchrotron radiation. Equation (53) can also be written as

$$N^2=1+\frac{4\chi}{\omega^2(2\bar{\Omega}^2-\omega^2)}\ , \tag{54}$$

where now the second term depends on χ. In this form the second term depends on plasma frequency through χ as defined in (A24) and through the effective frequency given by Eq. (51). If now we set $l=k_w$, the wiggler wave number, the function χ oscillates with respect to k_w as a Bessel function of the zeroth order. The evaluation of these functions under various conditions is given in Sec. IX.

VIII. POLARIZATION

The new polarization is given by

$$\mathbf{e}_{\lambda'}=\mathbf{e}_\lambda-\epsilon_3\frac{\mathbf{e}_\lambda\cdot\epsilon_1}{\mathbf{K}_\lambda\cdot\epsilon_3}l\ , \tag{55}$$

which in Cartesian coordinates becomes

$$e_{\lambda_1'}=e_{\lambda_1}+\frac{\Omega E}{\bar{\Omega}}\cos k_w z\ ,$$
$$e_{\lambda_2'}=e_{\lambda_2}+\frac{\Omega F}{\bar{\Omega}}\sin k_w z\ , \tag{56}$$
$$e_{\lambda_3'}=e_{\lambda_3}-\frac{\Omega_0}{\bar{\Omega}}F\ ,$$

with

$$F=-\frac{\Omega_0(e_{\lambda 1}\cos k_w z+e_{\lambda 2}\sin k_w z)+\Omega e_{\lambda 3}}{\Omega(K_{\lambda 1}\cos k_w z+K_{\lambda 2}\sin k_w z)-\Omega_0 K_{\lambda 3}}l\ , \tag{57}$$

where e_{λ_1}, e_{λ_2}, e_{λ_3}, K_{λ_1}, K_{λ_2}, and K_{λ_3} are initial polarization and initial wave vector components in the Cartesian system. If we now set $e_{\lambda_3}=0$ and $K_{\lambda_1}=K_{\lambda_2}=0$ initially, we then have

$$F=\frac{1}{K_\lambda}(e_{\lambda_1}\cos k_w z+e_{\lambda_2}\sin k_w z) \tag{58}$$

and

$$e_{\lambda_1'}=e_1(1+\alpha\cos^2 k_w z)+e_2\alpha\sin k_w z\cos k_w z$$
$$=e_1\left[1+\frac{\alpha}{2}\right]+\frac{\alpha}{2}e_\rho\cos(2k_w z-\theta)\ ,$$
$$e_{\lambda_2'}=e_1\alpha\sin k_w z\cos k_w z+e_2(1+\alpha\sin^2 k_w z) \tag{59}$$
$$=e_2\left[1+\frac{\alpha}{2}\right]+\frac{\alpha}{2}e_\rho\sin(2k_w z-\theta)\ ,$$
$$e_{\lambda_3'}=-\alpha\frac{\Omega_0}{\bar{\Omega}}(e_1\cos k_w z+e_2\sin k_w z)$$
$$=-\frac{\Omega_0}{\bar{\Omega}}e_\rho\cos(2k_w z-\theta)\ ,$$

where $\alpha=\dfrac{1\Omega}{K_\lambda\bar{\Omega}}$.

In the absence of the Wiggler field, $\alpha=0$ and the polarization is maintained as the original one; i.e., the axial magnetic field left to itself will introduce an additional polarization only in the Z direction. However, at points at which $2k_\omega z-\theta=\pi/4$ we get a circular polarization

condition, while at points where $2k_\omega z-\theta=(2n+1)\pi/2$ we have the modified polarization being plane polarized. At points where $2k_\omega z-\theta=n\pi$ we get a plane polarization in the X-Y plane with a finite axial component.

Solving the set of equations in (59) for e_1 and e_2 and imposing the condition $e_1^2+e_2^2=1$, we get an equation relating $e_{\lambda_1'}$ and $e_{\lambda_2'}$ as

$$(1+\alpha\overline{\alpha+2}\sin^2k_wz)e_{\lambda_1'}^2+(1+\alpha\overline{\alpha+2}\cos^2k_wz)e_{\lambda_2'}^2 -[2\alpha(\alpha+2)\sin k_wz\cos k_wz]e_{\lambda_1'}e_{\lambda_2'}=(1+\alpha)\ . \quad (60)$$

The associated determinant of Eq. (60) has the value $(1+\alpha)^2$, which is positive definite. Hence Eq. (60) it an equation for an ellipse and the emerging radiation is elliptically polarized. If now $e_{\lambda 2}=0$, i.e., if the incident beam is plane polarized, we still have an elliptically polarized beam with

$$\frac{e_{\lambda_1'}^2}{2(1+\alpha\cos^2k_\omega z)^2}+\frac{e_{\lambda_2'}^2}{2\alpha\sin^2k_\omega z\cos^2k_\omega z}\ . \quad (61)$$

IX. DISCUSSION

We shall discuss in this section the importance of the various relations evaluated in the previous sections. To calculate the different quantities, we shall define the different frequencies normalized to the synchrotron frequency due to the axial magnetic field. Thus

$$x=\frac{\nu_\lambda}{\Omega_0},\quad y=\frac{\omega_{\rm pl}}{\Omega_0},\quad z=\frac{\Omega}{\Omega_0}\ ,$$
$$u=\frac{1}{K_\lambda}\left[\frac{v_{\rm th}}{c}\right],\quad \frac{\beta\hbar\Omega_0}{2}=\left[\frac{\hbar\Omega_0}{mv_{\rm th}^2}\right]\ , \quad (62)$$

where $v_{\rm th}$ is the thermal velocity of the ambient plasma, $\beta=(kT)^{-1}$, T being temperature and k the Boltzmann constant. In terms of these variables we write

$$A^2=\frac{u^2}{4}\coth\left[\frac{\beta\hbar\Omega_0}{2}\right],$$
$$c=\frac{4\pi\sqrt{1+z^2}}{\sinh\dfrac{\beta\hbar\Omega_0}{2}}\left[\frac{(1-2\sqrt{\beta\hbar\Omega_0})}{\beta\hbar\Omega_0}\right], \quad (63)$$

and χ_0 as given in Eq. (A24) is written as

$$\frac{\chi_0}{\Omega_0^4}=c\,e^{-A^2x^2}J_0(xu/\sqrt{1+z^2})J_0\left[xu\frac{1+\sqrt{1+z^2}}{\sqrt{1+z^2}}\right] \times\frac{y^2(x^2+y^2)^{3/2}}{x^2+y^2-z^2-1}\ . \quad (64)$$

This enables us to define σ^2 as given in Eq. (41) as

$$\frac{\sigma^2}{\Omega_0^4}=(x^2+y^2-z^2-1)^2 4\frac{\chi(0)}{\Omega_0^4}\ , \quad (65)$$

and hence the effective frequency

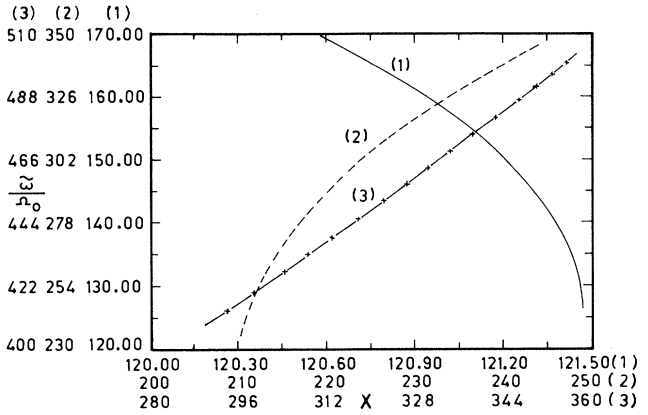

FIG. 7. A plot of the effective frequency ω as a function of the ambient radiation frequency normalized to the synchrotron frequency.

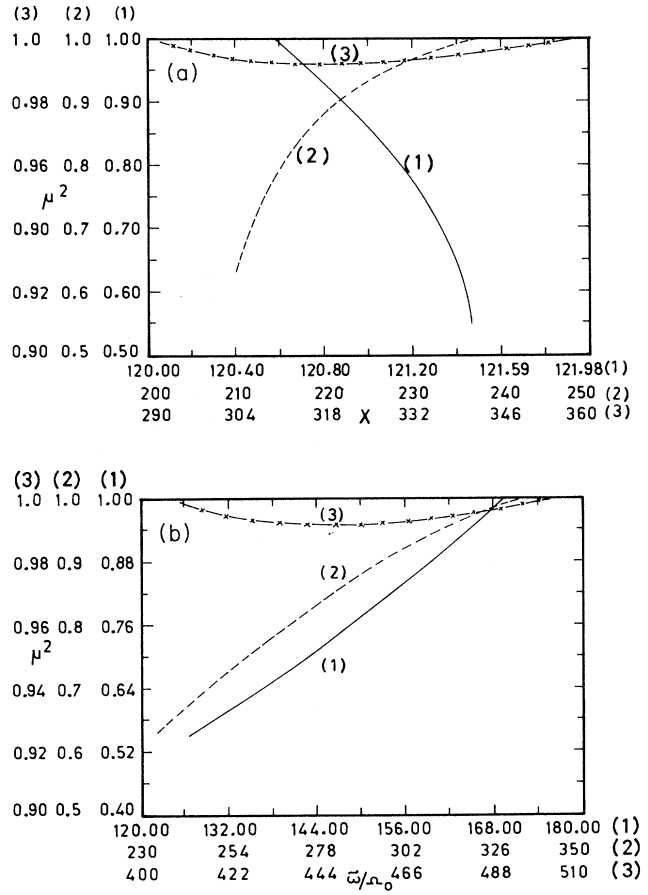

FIG. 8. A plot of μ^2 ($=\cos^2\theta$), θ being the semivertical angle of the Čerenkov cone (a) as a function of $X=v_\lambda/\Omega_0$ and (b) a function of ω/Ω_0 equal to the effective frequency. The solid curve for the first window, the slashed one is for second window, and the slashed-crossed one is for window 3. The amplitude and frequencies for the various windows are given on the Y and X axes.

TABLE I. Allowed ranges of frequencies (X), effective frequencies (ω/Ω_0), μ^2 square of the cosine of the Čerenkov angle (θ), refractive index (N^2) and power P. The last column indicate the total power contained in the frequency interval. These are evaluated for $c/v_A = 1.62$, v_A being the Alfvén velocity. The thermal velocity is taken as $0.1c$ ($=v_{th}$).

	X	ω/Ω_0	μ^2	θ	N^2	P	$\Delta p \Delta(\omega/\Omega_0)$
R_1	121.47	126.71	0.5441	42.5°	1.8383	57.78	2397
	120.58	169.59	0.9891	6°	1.0113	1.88	
R_2	210.0	234.28	0.6223	38°	1.6070	88.50	8355
	237.0	333.16	0.9881	6.3°	1.0121	4.00	
R_3	291.0	409.41	0.9897	6°	1.0104	4.23	84
	359.0	505.14	0.9899	6°	1.0102	5.11	

$$\frac{\omega}{\Omega_0} = \left[x^2+y^2+z^2+1+\frac{\sigma}{\Omega_0^2}\right]^{1/2} . \tag{66}$$

Having defined these different frequencies we now consider Eq. (49) for the Čerenkov angle. Equation (46) gives the cosine of this angle and this value lies between 0 and 1. Hence Eq. (49) gives a domain of validity for these angles, viz.

$$0 \le \frac{x^2+y^2+z^2+1+\dfrac{\sigma}{\Omega_0^2}}{2\beta_0^2(x^2+y^2)} \le 1 . \tag{67}$$

For a preassigned value of y ($=1.62$) and $Z=0.1$ and also $1/k=0.1$, and $v_{th}=0.1c$, relation (67) gives three allowed domains for x ($=120.58-121.47$; 210–237, and 291–359) through which emission takes place. The effective frequency ω/Ω_0 as a function of x for the above set of values is plotted in Fig. 7. The solid curve is for the first range, the slashed curve for the second domain, and the curve with slash and cross corresponds to the third window. It can be seen that the curvature continuously changes as the windows change, i.e., the slope at every point changes its sign from negative to positive for the different windows. Figure 8(a) is a plot of μ^2 as a function of x. Here again the above feature is evident in which for the third window the refractive index is almost unity, so much so that the system behaves almost as a vacuum for this window. Figure 8(b) is a plot of μ^2 as a function of the effective frequency ω/Ω_0. However, as the windows change, there is no change in the sign of the slope, but it decreases towards unity as the frequency increases, i.e., $\mu^2 \cong 1$, thereby giving the semivertical angle close to zero. Radiation in this range is therefore confined to a cone of very narrow apex angle. The corresponding angles are given in Table I. It may be seen that the higher frequencies are confined to the inner surface of the annular cone, while lower frequencies are confined to the periphery. Figures 9(a) and 9(b) give the plots of the refractive index as a function of x and ω/Ω_0. Here again, while the curves get drastically changed in their structure in Fig. 9(a), in Fig. 9(b) the refractive index steadily falls from a higher value to unity as the effective frequency increases, which implies that dispersion decreases with increasing frequency and the medium behaves like a vacuum for higher frequencies. Figures 10(a)and 10(b) are plots of emitted power as a function of x and ω/Ω_0. While as a function of x, the power structure is peculiar, the power shows a nonthermal structure with a negative slope as a function of the effective frequency. Again, total power is more in the middle window and is small for the higher window. Thus, as the window changes, radia-

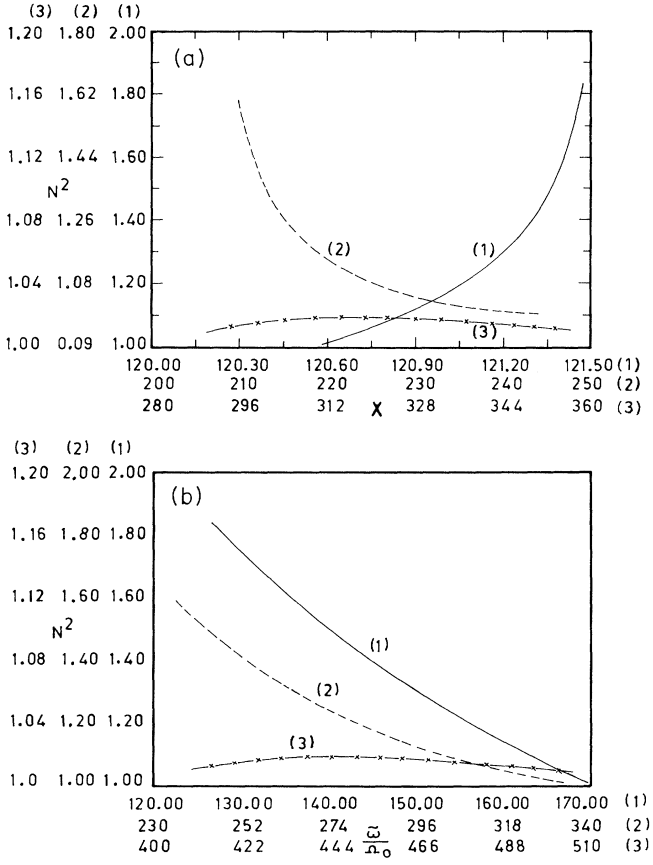

FIG. 9. Refractive index (square) of the plasma medium (a) as a function of X and (b) as a function of the effective frequency.

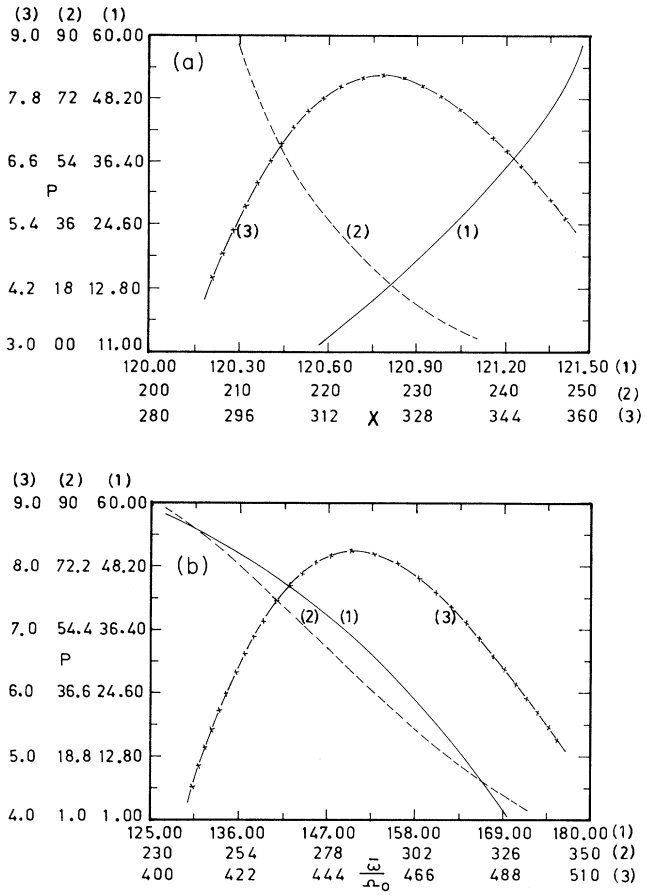

FIG. 10. The power output (a) as a function of X and (b) as functions of ω/Ω_0. All of these curves are with $y=1.02$, $z=0.1$.

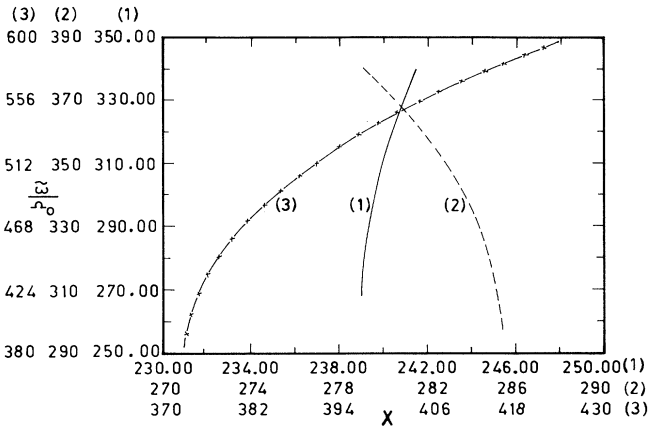

FIG. 11. Plot of ω/Ω_0 as a function of X for the three distinct allowed windows for $y=10$ which is the same as $\beta=1$.

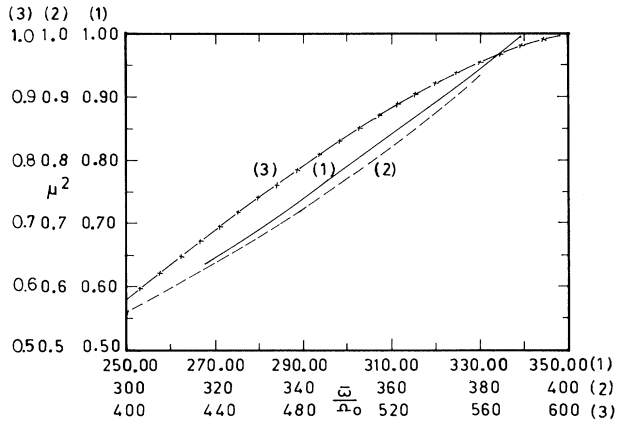

FIG. 12. The square of the cosine of the Čerenkov angle as a function of ω/Ω_0 in the second set of three windows ($y=10$).

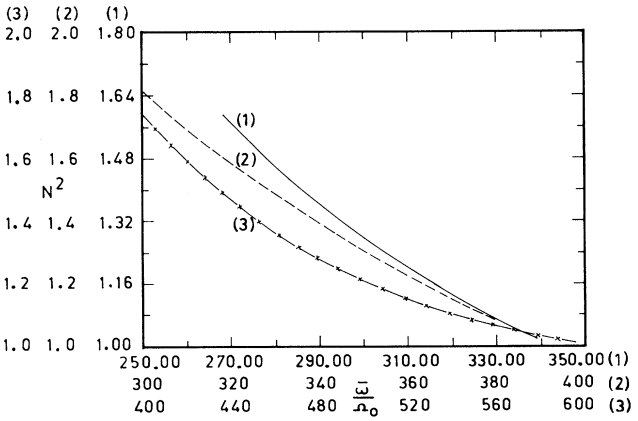

FIG. 13. A plot of the refractive index as a function of the effective frequency for the three windows.

tion power increases and decreases. Thus, in the above discussion, it become increasingly evident that one should consider the various quantities as functions of effective radiation frequency and that the ambient radiation acts only as a trigger to effect interaction in the spirit of the spontaneous emission. These results are presented in Table I.

To study the effect of plasma density on the emission mechanism, we repeated the above calculation for $y=10$ which corresponds to $(c/v_A)^2=10$, v_A being the Alfvén velocity. This defines a new frequency as $\nu_A^2=(ck_\omega)^2/10$). Figure 11 is a plot of ω/Ω_0 as a function of x. Compared with Fig. 7, the curves show completely different structure for this value of y, and also the range intervals are different. For the three ranges, concavity in Fig. (7) has changed to convexity in the present one.

Figure 12 is a plot of μ^2 as a function of ω/Ω_0. The three domains over which the inequality is satisfied are given in Table II. One could observe that in the first range, higher frequencies are radiated with a smaller semivertical angle, while the lower ones are radiated at the other periphery of the hollow cone. This trend is

TABLE II. The allowed ranges of frequencies when the ratio of the velocity of light to the Alfvén speed is 10. The various quantities are as defined in Table I, i.e., effective frequency (ω/Ω_0), Čerenkov angle θ, μ^2 ($=\cos^2\theta$), refractive index (N^2), power P, and total power (ΔP)[$\Delta(\omega/\Omega 0)$].

Range	X	ω/Ω_0	μ^2	θ	N^2	P (ergs/sec Hz)	$\Delta p \Delta(\omega/\Omega_0)$
R_1	239	268.14	0.6345	37°9′	1.5917	99.68	6761
	241	339.40	0.9525	12°34′	1.0143	4.80	
R_2	285	299.81	0.6059	38°42′	1.8133	134.47	8508
	279	379.88	0.9350	14°46′	1.0802	28.21	
R_3	373	383.97	0.5348	43°	1.8887	180.67	36 952
	424	596.40	0.9986	2°	1.0114	6.72	

again preserved in R_2 and R_3, as can be seen from Fig. 12. However, in the case of the refractive index, as given in Fig. 13, the function decreases to unity as the effective frequency increases. The dispersion decreases and the medium becomes more and more transparent with increasing frequency. As regards power, there is more power in the lower frequencies as compared to the higher ones, which is depicted in Fig. 14. There is very little power in the range R_3, while there is more power in the middle range. These features are also observed in Table I. In the case of $\beta=1$, power content increases as the range increases, which again has been seen in Table I. The results are collected in Table II.

The above two tables reveal another feature, viz., if we take the product of the difference in power and the effective frequency interval, in the first case it increases and then decreases, while in the second case it steadily increases. This gives the qualitative behavior of the integrated power in the given interval. To obtain this analytically would, however, be difficult.

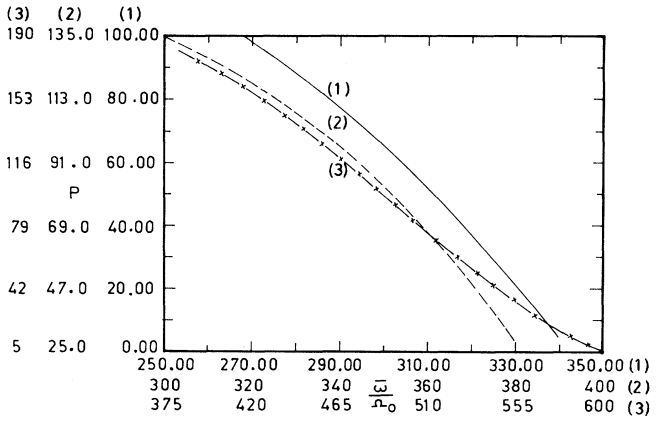

FIG. 14. Emitted power as a function of ω/Ω_0 for $y=10$. Again, the solid curve is for the first window, the slashed one is for the second, and the slash and cross is for the outermost window.

X. CONCLUSIONS

The main conclusion in this paper are (a) radiation is confined to a set of concentric Čerenkov cones, and these cones travel along a helical path, with its guiding center being confined to an undulating magnetic-field line. This poses the cone towards the observer at regular intervals, giving what is generally known as the searchlight effect. If we identify the wiggler as formed by Alfvén waves, then the frequency of emission observed would be a function of this frequency as well. The argument of the Bessel function has the term lp_0, where l is the wave number and p_0 is the Z component of the momentum, all being dimensionless. If we now take

$$lp_0=\sqrt{\hbar/m\Omega_0}\tilde{l}\frac{\tilde{P}_0}{\sqrt{m\hbar\Omega}}=\frac{l\tilde{P}_0}{m\Omega_0},$$

where $\tilde{l}$ and $\tilde{p}_0$ have dimension and are identified as $\tilde{l}=k_\omega$ and $\tilde{p}_0=mV_A$, V_A being the Alfvén velocity, we then have $lp_0=(k_\omega V_A)/\Omega_0$, where $k_\omega V_A$ is the Alfvén frequency. This could be a plausible explanation for the periodic emissions from astrophysical objects. (b) The full nonlinear effects, when taken into account, give a growth structure for the power spectrum which is explicitly shown in model calculations. The plasma density at the emitting source plays a crucial role in determining the frequency windows, indicating the existence of allowed and forbidden frequency ranges. (c) The refractive index is always greater than unity, as is expected for a Čerenkov process. (d) The power spectrum is nonthermal, as has been observed in the case of pulsars. (e) The nonlinear radiation as well as the curvature radiation produce a series of synergic frequencies (f). We have identified a natural coordinate system for the plasma embedding an axial and wiggler magnetic fields.

ACKNOWLEDGMENT

One of us (R.P.) would like to thank the Director of the IIA for hospitality extended to him during the tenure of this work.

APPENDIX: EVALUATION OF RESPONSE FUNCTION $\mathcal{E}(z)$

We take the first nonzero matrix element and we evaluate the average energy. The first propagator becomes unity, and we get the term e^2, the leading term in the series, as

$$\rho_t^{(1)}=\left[\frac{8\pi e^2}{V}\right]\int_0^t dt_1\int_0^{t_1}dt_2\frac{\partial}{\partial u}\cdot[\mathbf{e}_\lambda(\mathbf{e}_{\lambda'}\cdot\bar{\boldsymbol{\beta}})\cos(\mathbf{k}_\lambda\cdot\mathbf{q}_T)\cos(\mathbf{K}_{\lambda'}\cdot\mathbf{q}_T+\phi)e^{-\mathcal{L}t_2}\rho_T(0)]\oint dz\,e^{-iz(t_1-t_2)}u(z)\,, \tag{A1}$$

where now

$$u(z)=\frac{iz}{z^2-\bar{\nu}_\lambda^2}\,,$$

$$\bar{\boldsymbol{\beta}}=\boldsymbol{\beta}\cos\omega t_{12}+\boldsymbol{\beta}\times\boldsymbol{\epsilon}_3\sin\omega t_{12}+\boldsymbol{\epsilon}_3(\boldsymbol{\beta}\cdot\boldsymbol{\epsilon}_3)(1-\cos\omega t_{12})\,,$$

$$\phi=\frac{\alpha\Omega_0}{\omega}[\mathbf{e}_3\cdot\boldsymbol{\beta}\times\mathbf{K}_\lambda(1-\cos\omega t_{12})-\mathbf{K}_\lambda\cdot\boldsymbol{\beta}\sin\omega t_{12}+(\boldsymbol{\epsilon}_3\cdot\mathbf{K}_\lambda)(\boldsymbol{\epsilon}_3\cdot\boldsymbol{\beta})(\sin\omega t_{12}-\omega t_{12})]\,, \tag{A2}$$

with

$$t_{12}=t_1-t_2,\quad \omega=\frac{\bar{\Omega}}{\gamma},\quad \alpha=\frac{mc^2}{\hbar\Omega_0}\,.$$

If we now add the $-\lambda$ part, we get

$$\rho_{(t)}^{(1)}=\left[\frac{8\pi e^2}{V}\right]\int_0^t dt_1\int_0^{t_1}dt_2\frac{\partial}{\partial \mathbf{u}}\cdot[\mathbf{e}_\lambda(\mathbf{e}_{\lambda'}\cdot\bar{\boldsymbol{\beta}})\cos[(\mathbf{K}_{\lambda'}-\mathbf{K}_\lambda)\cdot\mathbf{q}_T+\phi)]e^{-\mathcal{L}t_2}\rho_T(0)\oint dz\,e^{-izt_{12}}u(z)\,. \tag{A3}$$

The next term in the series is

$$\rho^{(2)}=\left[\frac{8\pi e^2}{V}\right]\int_0^t dt_1\int_0^{t_1}dt_2\frac{\partial}{\partial \mathbf{u}}\cdot\{\mathbf{e}_\lambda(e_{\lambda'}\cdot\bar{\boldsymbol{\beta}})\cos[(K_{\lambda'}-\mathbf{K}_\lambda)\cdot q_T+\phi]e^{-\mathcal{L}t_2}\rho_T(0)\}\oint dz\,e^{-izt_{12}}u(z)\Delta(z)\,, \tag{A4}$$

where

$$\Delta(z)=\int dz\,e^{izt_{12}}\left[\frac{8\pi e^2}{mV\bar{\nu}_{\lambda'}}\right]\int_0^{t_2}dt_3\int_0^{t_3}dt_4\sin\bar{\nu}_\lambda t_{34}\int d\mathbf{P}_l d\mathbf{q}_l\{(\mathbf{e}_\lambda\cdot\mathbf{P}_l)(\mathbf{e}_{\lambda'}\cdot\mathbf{K}_\lambda)\sin[(\mathbf{K}_{\lambda'}-\mathbf{K}_\lambda)\cdot\mathbf{q}_1+\phi]$$

$$+m\bar{\Omega}\mathbf{e}_\lambda\cdot\boldsymbol{\epsilon}_3\times\mathbf{e}_{\lambda'}\cos[(\mathbf{K}_{\lambda'}-\mathbf{K}_\lambda)\cdot\mathbf{q}_l+\phi]\}e^{-\mathcal{L}t_3}\rho_l(0)\,, \tag{A5}$$

with

$$\phi=\frac{\Omega_0}{\bar{\Omega}}[-(\mathbf{K}_\lambda\cdot\mathbf{P}_l)\sin\bar{\Omega}t_{23}+\boldsymbol{\epsilon}_3\cdot\mathbf{P}_l\times\mathbf{K}_\lambda(1-\cos\bar{\Omega}t_{23})\,.$$

$$+K_3P_3(\sin\bar{\Omega}t_{23}-\bar{\Omega}t_{23})]\,. \tag{A6}$$

We now take an initial state constructed out of the wave functions of the unperturbed part of the Hamiltonian as

$$\rho_l(0)=\sum_n e^{-(P_2+\xi)^2}\frac{H_n^2(P_2+\xi)}{2^n n!\sqrt{\pi}}$$

$$\times\delta(P)\delta(P_3-P_3^0)e^{-\beta E_n}\delta(\eta)\delta(\zeta)\,, \tag{A7}$$

where $E_n=(n+1/2)\hbar\Omega_0$. (A8)

On operating with $e^{-\mathcal{L}t_3}\rho_T(0)$ we have

$$e^{-\mathcal{L}t_3}\rho(0)=\sum_n e^{-X^2}\frac{H_n^2(X)}{2^n n!\sqrt{\pi}}\delta(P-P_0)\delta(P_3-P_3^0)$$

$$\times e^{-\beta E_n}\delta(\eta)\delta(\zeta)\,, \tag{A9}$$

where

$$X=\xi+P_2-\left[1-\frac{\Omega_0}{\bar{\Omega}}\right]P(\sin(\bar{\Omega}t_3-\theta)+\sin\theta)\,. \tag{A10}$$

We shall now impose a wave vector conservation

$$\mathbf{K}_{\lambda'}=\mathbf{K}_\lambda+\boldsymbol{\epsilon}_1 l\,, \tag{A11}$$

which gives

$$\mathbf{e}_{\lambda'}=\mathbf{e}_\lambda-\mathbf{e}_b\frac{(\mathbf{e}_\lambda\cdot\mathbf{e}_1)}{(\mathbf{K}_\lambda\cdot\boldsymbol{\epsilon}_3)}l \tag{A12}$$

such that $\mathbf{e}_{\lambda'}\cdot\mathbf{K}_{\lambda'}=0$. We shall now perform the ξ integration, which is the same as X integration, and we then have Eq. (A5) as

$$\Delta(z)=\int dZ\, e^{izt_{12}}\left[\frac{8\pi e^2}{mV\bar{\nu}_{\lambda'}}\right]\int_0^{t_2}dt_3\int_0^{t_3}dt_4\sin\bar{\nu}_{\lambda'}t_{34}$$
$$\times\int d\mathbf{P}_l[(\mathbf{e}_\lambda\cdot\mathbf{P}_l)(\mathbf{e}_{\lambda'}\cdot\mathbf{K}_\lambda)\sin\bar{\phi}+m\bar{\Omega}(\mathbf{e}_\lambda\cdot\boldsymbol{\epsilon}_3\times\mathbf{e}'_\lambda)\cos\bar{\phi}]$$
$$\times L_n\left[\frac{l^2}{2}\right]e^{-l^2/4}e^{-\beta E_n}\delta(P-P_0)\delta(P_3-P_3^0)\,, \tag{A13}$$

where L_n are Laguerre polynomials and

$$\bar{\phi}=P\left\{\frac{\Omega_0}{\bar{\Omega}}[-(K_{\lambda_1}\cos\theta+K_{\lambda_2}\sin\theta)\sin\bar{\Omega}t_{23}+(K_{\lambda_2}\cos\theta-K_{\lambda_1}\sin\theta)(1-\cos\bar{\Omega}t_{23})]+1\left[\left[1+\frac{\Omega_0}{\bar{\Omega}}\right](\sin(\bar{\Omega}t_3-\theta)+\sin\theta)\right]\right\}. \tag{A14}$$

We shall now sum over the Landau levels using the generating functions for the Laguerre polynomials and write, say,

$$\sum_n L_n\left[\frac{l^2}{2}\right]e^{-l^2/4}e^{-\beta\hbar\Omega_0(n+1/2)}=\frac{-\frac{l^2}{e^4}\coth\frac{\beta\hbar\Omega_0}{2}}{2\sinh\frac{\beta\hbar\Omega_0}{2}}=\Gamma\,. \tag{A15}$$

We can then write Eq. (A13) as

$$\Delta(z)=-\left[2\frac{\omega_{\rm pl}^2}{\bar{\nu}_{\lambda'}}\Gamma l\right]\int dz\, e^{izt_{12}}\int_0^{t_2}dt_3\int_0^{t_3}dt_4\sin\bar{\nu}_{\lambda'}t_{34}\int dP_l(\mathbf{e}_\lambda\cdot\mathbf{P}_l)(\mathbf{e}_\lambda\cdot\boldsymbol{\epsilon}_l)\sin(\bar{\phi})\delta(P-P_0)\delta(P_3-P_3^0)\,, \tag{A16}$$

where we have used Eq. (A12) and again summed up over 1 giving an N which in the thermodynamic limit N/V gives a concentration resulting in the plasma frequency $\omega_{\rm pl}^2$ $(=4\pi ne^2/m)$.

We shall now sum over the polarization vector using the relation

$$(\mathbf{e}_\lambda\cdot\mathbf{a})(\mathbf{e}_\lambda\cdot\mathbf{b})=\frac{(\mathbf{K}_\lambda\times\mathbf{a})\cdot(\mathbf{K}_\lambda\times\mathbf{b})}{K_\lambda^2} \tag{A17}$$

and write

$$\Delta(z)=-2\left[\frac{\omega_{pl}^2\Gamma l}{\bar{\nu}_{\lambda'}}\right]\int dz\, e^{izt_{12}}\int_0^{t_2}dt_3\int_0^{t_3}dt_4\sin\bar{\nu}_{\lambda'}t_{34}\int P_l dP_l d\theta\, dP_3\left[P_1-\frac{\mathbf{K}_{\lambda_1'}\cdot(\mathbf{K}_\lambda\cdot\mathbf{P}_l)}{K_\lambda^2}\right]$$
$$\times\sin(\bar{\phi})\delta(P-P_0)\delta(P_3-P_3^0)\,, \tag{A18}$$

where now

$$\bar{\phi}=-2\frac{\Omega_0}{\bar{\Omega}}PK_4\sin\theta_k\sin\frac{\bar{\Omega}t_{23}}{2}\cos\left[\phi_k-\theta_p+\frac{\bar{\Omega}t_{23}}{2}\right]-K_{3\lambda}P_3\Omega_0t_{23}+1PA\,\sin(\theta_p-\alpha)\,, \tag{A19}$$

where

$$A^2=\left[\frac{\Omega_0}{\bar{\Omega}}\right]^2+\left[1+\frac{\Omega_0}{\bar{\Omega}}\right]^2-2\left[\frac{\Omega_0}{\bar{\Omega}}\right]\left[1+\frac{\Omega_0}{\bar{\Omega}}\right]\cos\bar{\Omega}t_3\,. \tag{A20}$$

After performing the integration with respect to P, P_3, and θ_p we have

$$\Delta(z)=\frac{\chi(z)}{(z^2-\bar{\nu}_\lambda^2)(z^2-\bar{\Omega}^2)}\,, \tag{A21}$$

where

$$\chi(z)=\left[2\omega_{\rm pl}^2\left[\frac{\Omega_0}{\overline{\Omega}}\right]\left[1+\frac{\Omega_0}{\overline{\Omega}}\right]P_0(P_0-2)\frac{e^{-l^2/4}\cosh[(\beta\hbar\Omega_0/2]}{\sinh(\beta\hbar\Omega_0)/2}\right]$$
$$\times\left[\sum_n \epsilon_n J_n\left[\frac{\Omega_0}{\overline{\Omega}}P_0 l\right]J_n((1+\frac{\Omega_0}{\overline{\Omega}})P_0 l)\overline{\Omega}\bar{v}_\lambda\right]$$
$$\times\left[\frac{(n+1[3z^2+(n+1)\overline{\Omega}]^2-\bar{v}_\lambda^2)(z^2-\bar{v}_\lambda^2)(z^2-\overline{\Omega}^2)}{\{z^2-[(n+1)\overline{\Omega}]^2\}\{z^2-[(n+1)\overline{\Omega}-\bar{v}_\lambda]^2\}\{z^2-[(n+1)\overline{\Omega}+\bar{v}_\lambda]^2\}}\right.$$
$$\left.-\frac{(n-1)\{3z^2+[(\overline{n-1})\overline{\Omega}]^2-\bar{v}_\lambda^2\}(z^2-\bar{v}_\lambda^2)(z^2-\overline{\Omega}^2)}{\{z^2-[(\overline{n-1})\overline{\Omega}]^2\}\{z^2-[(\overline{n-1})\overline{\Omega}+\bar{v}_\lambda]^2\}\{z^2-[(\overline{n-1})\overline{\Omega}-\bar{v}_\lambda]^2\}}\right]. \quad \text{(A22)}$$

In evaluating these integrals, we had obtained $J_0(P_0 A)$, A being given by Eq. (A20), and this was expanded using the addition theorem in the Bessel function and the most dominated terms in Eq. (22) when taking the Marconian limit (i.e., $t\to\infty$ or $Z\to 0$). We get

$$\Delta(z)=\frac{\chi(0)}{(z^2-\bar{v}_\lambda^2)(z^2-\overline{\Omega}^2)}, \quad \text{(A23)}$$

where now

$$\chi(0)=+\left[4\pi\omega_{\rm pl}^2\Omega_0\left[1+\frac{\Omega_0}{\overline{\Omega}}\right]\frac{\bar{v}_\lambda^3}{\bar{v}_\lambda^2-\overline{\Omega}^2}P_0(P_0-2)\Gamma\right]$$
$$\times J_0\left[lP_0\frac{\Omega_0}{\overline{\Omega}}\right]J_0(lP_0(1+\Omega_0/\overline{\Omega})). \quad \text{(A24)}$$

This completes the evaluation of the response function.

*Department of Physics, Cochin University of Science & Technology, Cochin 682 022, India.

[1] J. M. Rankin, Astrophys. J. **274**, 333 (1983); **274**, 358 (1983); **301**, 901 (1986); **352**, 247 (1990); **352**, 258 (1990).
[2] J. M. Rankin, D. R. Stinebring, and I. M. Weisberg, Astrophys. J. **346**, 869 (1989).
[3] V. Radhakrishnan and D. J. Cooke, Astrophys. Lett. **3**, 225 (1969).
[4] V. S. Bestin, A. V. Gurevich, and Ya. N. Istomin, Appl. Space Sci. **146**, 205 (1988).
[5] R. G. Little John, A. N. Kauffman, and G. I. Johnston, Phys. Lett. A **120**, 291 (1987).
[6] R. Pratap and A. Sen, Phys. Rev. A **42**, 7395 (1990).
[7] R. Pratap and A. Sen, Phys. Rev. A **45**, 2593 (1992).
[8] R. Balescu, *Equilibrium & Nonequilibrium Statistical Mechanics* (Wiley-Interscience, New York, 1975).
[9] J. Schwinger, Wu-Yang Tsai, and T. Erber, Ann. Phys. **96**, 303 (1976).
[10] D. N. Patro, Phys. Rev. Lett. **49**, 1083 (1982).
[11] D. N. Patro and R. Pratrap, Physica **117A**, 189 (1983).
[12] L. Fujiwara, Prog. Theor. Phys. **7**, 433 (1952).
[13] I. M. Frank and I. G. Tamm, Dokl. Akad. Nauk SSSR **14**, 109 (1937).